AD-A145 510 DESIGN MANUFACTURE AND TESTING OF COMPLIANT COATINGS FOR REDUCTION OF TUR..(U) DAVID W TAYLOR NAVAL SHIP RESEARCH AND DEVELOPMENT CENTER BET..

1/1

UNCLASSIFIED S C DICKINSON ET AL. AUG 84 DTNSRDC-84/060 F/G 11/3 NL

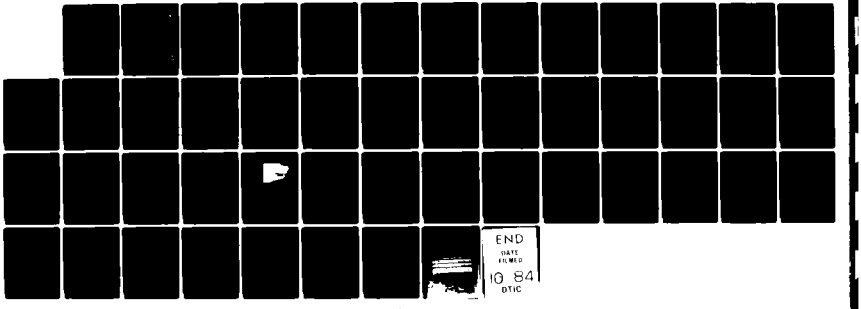

END
DATE FILMED
10 84
DTIC

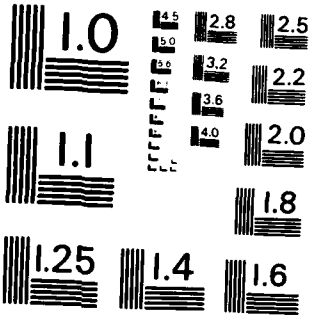

(12)

DTNSRDC-84/060

AD-A145 510

DAVID W. TAYLOR NAVAL SHIP RESEARCH AND DEVELOPMENT CENTER

Bethesda, Maryland 20084

DESIGN, MANUFACTURE, AND TESTING OF COMPLIANT COATINGS FOR REDUCTION OF TURBULENT DRAG

by

Stuart C. Dickinson
John L. Power
John J. Eynck

APPROVED FOR PUBLIC RELEASE: DISTRIBUTION UNLIMITED

SHIP PERFORMANCE DEPARTMENT
RESEARCH AND DEVELOPMENT REPORT

August 1984

DTNSRDC-84/060

DESIGN, MANUFACTURE, AND TESTING OF COMPLIANT COATINGS FOR REDUCTION OF TURBULENT DRAG

MAJOR DTNSRDC ORGANIZATIONAL COMPONENTS

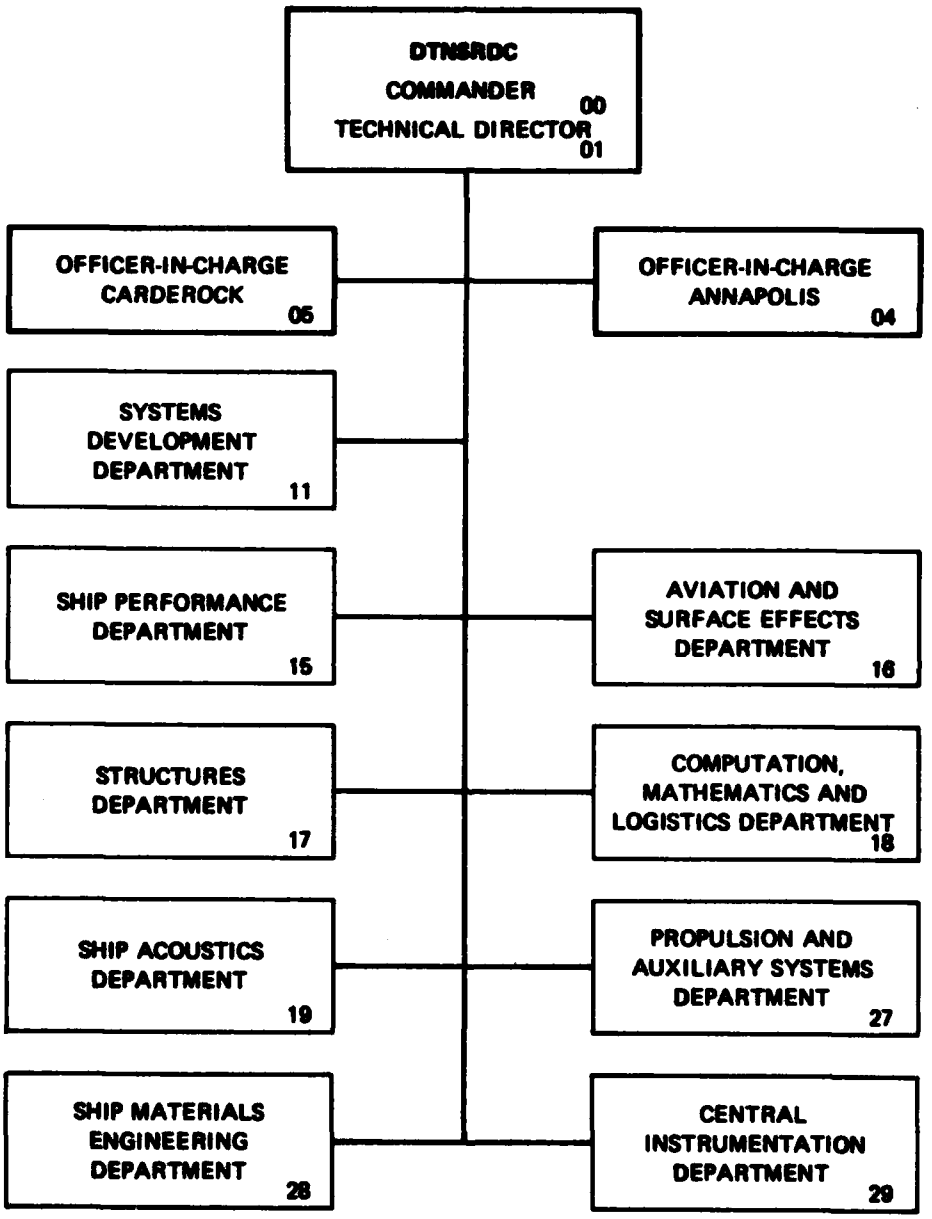

UNCLASSIFIED

SECURITY CLASSIFICATION OF THIS PAGE *(When Data Entered)*

REPORT DOCUMENTATION PAGE		READ INSTRUCTIONS BEFORE COMPLETING FORM
1. REPORT NUMBER DTNSRDC-84/060	2. GOVT ACCESSION NO. AD-A145 540	3. RECIPIENT'S CATALOG NUMBER
4. TITLE *(and Subtitle)* DESIGN, MANUFACTURE, AND TESTING OF COMPLIANT COATINGS FOR REDUCTION OF TURBULENT DRAG		5. TYPE OF REPORT & PERIOD COVERED Formal 6. PERFORMING ORG. REPORT NUMBER
7. AUTHOR(s) Stuart C. Dickinson John L. Power John J. Eynck		8. CONTRACT OR GRANT NUMBER(s)
9. PERFORMING ORGANIZATION NAME AND ADDRESS David W. Taylor Naval Ship Research and Development Center Bethesda, Maryland 20084		10. PROGRAM ELEMENT, PROJECT, TASK AREA & WORK UNIT NUMBERS Program Element 61153N Project 02301 Work Unit 1542-223
11. CONTROLLING OFFICE NAME AND ADDRESS Office of Naval Research (Code 432) Arlington, Virginia 22217		12. REPORT DATE August 1984 13. NUMBER OF PAGES 45
14. MONITORING AGENCY NAME & ADDRESS*(if different from Controlling Office)*		15. SECURITY CLASS. *(of this report)* UNCLASSIFIED 15a. DECLASSIFICATION/DOWNGRADING SCHEDULE

16. DISTRIBUTION STATEMENT *(of this Report)*

APPROVED FOR PUBLIC RELEASE: DISTRIBUTION UNLIMITED

17. DISTRIBUTION STATEMENT *(of the abstract entered in Block 20, if different from Report)*

18. SUPPLEMENTARY NOTES

19. KEY WORDS *(Continue on reverse side if necessary and identify by block number)*

Drag Reduction
Compliant Coating
Turbulent Boundary Layer
Static Divergence
Fluid-Compliant Surface Interaction
Impedance Matching

20. ABSTRACT *(Continue on reverse side if necessary and identify by block number)*

The drag of three compliant coatings was measured in the DTNSRDC 36-inch water tunnel. Two coatings were of the "Kramer" type, while the other one was a closed-cell neoprene foam. The drag of the 2.032-m (80-in.) long and 0.737-m (29-in.) wide compliant coatings was compared to the drag of a smooth, solid reference plate.

(Continued on reverse side)

DD FORM 1 JAN 73 1473 EDITION OF 1 NOV 65 IS OBSOLETE
S/N 0102-LF-014-6601

UNCLASSIFIED
SECURITY CLASSIFICATION OF THIS PAGE *(When Data Entered)*

(Block 20 continued)

The first Kramer coating failed at 9.14 m/s (30 ft/sec). Improved fabrication of the second Kramer coating allowed free-stream velocities up to the 18.3 m/s (60 ft/sec) tunnel top speed without failure. The drag of the Kramer coating was within the 2% rms scatter of the smooth, solid plate drag at all velocities tested.

The surface of the closed-cell neoprene foam was rough, and the drag was 14-20% higher than the smooth, solid plate at low velocities. At about 12.2 m/s (40 ft/sec), transverse waves appeared in the coating, and the drag rapidly increased with increasing velocity. The appearance of the static divergence waves occurred at a nondimensional velocity $V/(G/\rho)^{1/2} = 1.9$, where V is the free-stream velocity, ρ is the water density, and G is the shear modulus of the foam.

A method designed to match the dynamic properties of a turbulent boundary layer with the mechanical properties of a compliant wall is introduced. The objective of this approach is to produce passive coatings from existing materials which may reduce the turbulent shear stress at high Reynolds numbers.

A "turbulence impedance" is developed from the magnitude and frequency of the pressures in the boundary layer and from the allowable deformation of the compliant surface. This impedance is equated to the specific acoustic impedance of the compliant wall. Such a matching may allow efficient energy transfer across the fluid/solid interface, thereby modifying the turbulence. Three possible regions of impedance matching are examined, with discussion of the favorable as well as detrimental aspects of each case. Static divergence causes roughness and increased drag and is included as a constraint on the properties of the compliant wall.

TABLE OF CONTENTS

LIST OF FIGURES

NOTATION

A	Area of test plate
b	Width of test plate
C_{D_L}	Drag coefficient based on total drag
C_{D_2}	Drag coefficient based on test plate drag
c_τ	Local skin friction coefficient
D_L	Smooth plate drag from nose to end of test plate
D_1	Drag of nose section
D_2	Drag of test plate
G	Shear modulus
K	Dynamic stiffness
K_a	Admissible roughness of a hydraulically smooth surface
L	Length from nose to end of test plate
ℓ_1	Length of nose section
ℓ_2	Length of test plate
N	Newton
$\hat{n}$	Unit vector normal to surface
P'	Significant pressure fluctuations
R_L	Reynolds number based on L
R_{ℓ_1}	Reynolds number based on ℓ_1
R_X	Reynolds number based on X
T	Thickness of coating

$\underline{U}$	Wall velocity
U_∞	Free-stream velocity
u	Local velocity
$\underline{u}$	Fluid velocity
X	Local distance measured from nose
Z_A	Specific acoustic impedance
Z_T	Turbulence impedance
δ	Boundary layer thickness
$\overline{\lambda}$	Wall flow length scale
ν	Kinematic viscosity of fluid
ρ_c	Density of coating
ρ_w	Density of water
τ	Local skin friction
ω	Frequency of significant pressure fluctuations
ω_o	Resonance frequency of coating

ACRONYMNS

NACA	National Advisory Committee for Aeronautics
psia	Pounds per square inch (absolute)
rms	Root mean square
shp	Shaft horsepower
VPWT	Variable Pressure Water Tunnel

ABSTRACT

The drag of three compliant coatings was measured in the DTNSRDC 36-inch water tunnel. Two coatings were of the "Kramer" type, while the other one was a closed-cell neoprene foam. The drag of the 2.032-m (80-in.) long and 0.737-m (29-in.) wide compliant coatings was compared to the drag of a smooth, solid reference plate.

The first Kramer coating failed at 9.14 m/s (30 ft/sec). Improved fabrication of the second Kramer coating allowed free-stream velocities up to the 18.3 m/s (60 ft/sec) tunnel top speed without failure. The drag of the Kramer coating was within the 2% rms scatter of the smooth, solid plate drag at all velocities tested.

The surface of the closed-cell neoprene foam was rough, and the drag was 14-20% higher than the smooth, solid plate at low velocities. At about 12.2 m/s (40 ft/sec), transverse waves appeared in the coating, and the drag rapidly increased with increasing velocity. The appearance of the static divergence waves occurred at a nondimensional velocity $V/(G/\rho)^{1/2} = 1.9$, where V is the free-stream velocity, ρ is the water density, and G is the shear modulus of the foam.

A method designed to match the dynamic properties of a turbulent boundary layer with the mechanical properties of a compliant wall is introduced. The objective of this approach is to produce passive coatings from existing materials which may reduce the turbulent shear stress at high Reynolds numbers.

A "turbulence impedance" is developed from the magnitude and frequency of the pressures in the boundary layer and from the allowable deformation of the compliant surface. This impedance is equated to the specific acoustic impedance of the compliant wall. Such a matching may allow efficient energy transfer across the fluid/solid interface, thereby modifying the turbulence. Three possible regions of impedance matching are examined, with discussion of the favorable as well as detrimental aspects of each case. Static divergence causes roughness and increased drag and is included as a constraint on the properties of the compliant wall.

ADMINISTRATIVE INFORMATION

The work described in this report was performed at the David W. Taylor Naval Ship Research and Development Center (DTNSRDC) and was funded under the Office of Naval Research's Compliant Coating Drag Reduction Program, Program Element 61153N, Project 02301, and Work Unit 1542-223.

INTRODUCTION

The boundary layer flow over most of the surface area of marine vehicles is turbulent. The ability to delay the laminar/turbulent transition for small vehicles, or to reduce the turbulent drag forces for large vehicles, is highly desirable from both the powering and acoustic points of view. Because most vehicles have space and powering constraints, only passive drag reduction techniques will be considered, specifically compliant hull coatings. Here "passive" is used in the context of not requiring any energy or material input from the vehicle systems. Because passive compliant coatings do respond to the local flow conditions, under some conditions it may be possible to design a coating which reduces drag in a fully developed turbulent boundary layer. At present, many researchers are being sponsored by the Office of Naval Research (ONR) Compliant Coating Drag Reduction Programs to study the stabilizing effects of passive compliant coatings and the delay of transition.[1*]

The first reports of compliant coating drag reduction (in water) were made by Max Kramer.[2-5] Since then, there have been several publications reporting drag reduction; however, none of these has been verifiable. Kramer attributed his success to a delay in laminar-to-turbulent transition in the boundary layer, whereas our objective is to reduce the drag of the fully turbulent boundary layer at Reynolds numbers typical of large marine vehicles. Recent investigations involving drag measurements of turbulent flow over compliant surfaces were conducted by Klebanoff, Mease, and Rowland[6] at the National Bureau of Standards, and by Rathsom et al.[7] at the Naval Ocean Systems Center.

The expertise and special facilities at the David W. Taylor Naval Ship Research and Development Center (DTNSRDC) have allowed a multidisciplinary approach to the design, manufacture, and testing of compliant coatings. The Hydrodynamics Branch is able to design and test the coatings, while the Plastics and Rubber Branch can formulate and produce the materials. Drag experiments are conducted in a high-speed water tunnel using an existing flat-plate dynamometer modified to accept compliant coatings; drag measurements are made in the length Reynolds number range of 1.8×10^7 to 5.5×10^7. During the present investigation, we have attempted to reproduce Kramer's three-layer solid coating as well as to design new coatings. This report describes both Kramer and foam-type coatings that were produced and tested in fully turbulent boundary layers. An impedance-matching-type calculation,

---

*A complete listing of references is given on page 37.

described below, was devised for the design of drag-reducing compliant coatings, but not in time to influence the choice of the tested foam coating. This report covers the manufacture and testing of the three coatings and then presents the design method hypothesized for future coatings.

An impedance matching calculation is developed for the design of future drag reducing compliant coatings. A quick examination of the hypothesized compliant coating drag reduction mechanism illuminates the difficulty of achieving a practical surface. The fluctuating pressures in the turbulent boundary layer will deform the compliant surface, changing the boundary conditions experienced by the fluid. If there is any possibility of drag reduction by passive compliant coatings, this change of boundary conditions is likely to interact favorably with the structure of the wall turbulence. For a given configuration, the fluctuating pressures increase with an increase in Reynolds number. However, one must maintain a hydraulically smooth surface on the coating or else the deformation will increase the drag, as would roughness. The allowable deformation amplitude, therefore, decreases with increasing Reynolds number. Thus, an optimum coating can be expected to perform well only at one (or a limited range of) Reynolds number. The results of the impedance matching calculations should identify regions of strong response of the coating to the turbulent boundary layer, where the drag will either increase or decrease, thus guiding experimental investigations.

MATERIAL PRODUCTION AND PROPERTIES

Three compliant coatings were produced for testing in the 36-in. water tunnel. Two were of the multilayer Kramer type, and the third was made of a closed-cell foam. All of the coatings were applied to aluminum panels 2.08-m (80 in.) long by 0.74-m (29 in.) wide. The panels were sandblasted prior to application of an adhesive primer in order to enhance the rubber-to-metal substrate bond. Different assembly techniques and procedures were developed for each of the compliant coatings.

The first compliant coating, which was built for testing in August 1981, was a Kramer-type coating comprised of a neoprene layer, a natural rubber layer, and a paint layer. The bottom layer of Neoprene W (1.02 mm [0.040 in.] thick) was provided by Dr. W. Madigosky[8] of the Naval Surface Weapons Center. The neoprene was produced in approximately 1 ft squares (0.93 m^2) which were then pieced together on the aluminum panel. This area was then covered by a 0.38-mm (0.015 in.) thick

natural rubber layer, and the two layers were glued using a solvent-based adhesive. Floquil R10 paint was sprayed on the top to produce a three-layer coating (see Figure 1). The specified paint, however, is manufactured with a grit content (to produce a nonreflective surface) which produces a surface roughness greater than 300 μin. rms. This surface roughness is known to increase drag at the Reynolds numbers tested, so the paint layer was smoothed by wet sanding.

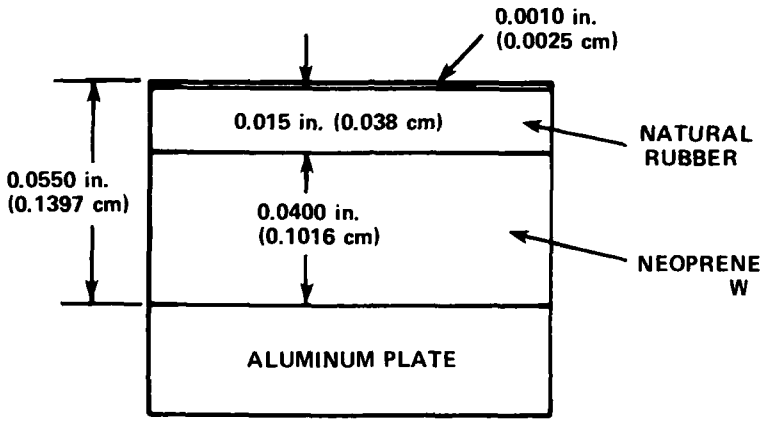

Figure 1a - Kramer Coating

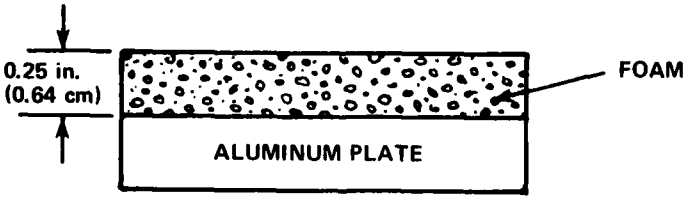

Figure 1b - Foam Coating

Figure 1 - Diagram of Coatings Tested

The second Kramer-type coating consisted of a 1.02-mm (0.040-in.) thick ultra-soft Neoprene GRT layer covered by a 0.38-mm (0.015-in.) thick natural gum rubber layer. The neoprene layer was produced at the DTNSRDC Annapolis Laboratory. A Monsanto Oscillating Disc Rheometer was used to obtain curing times and temperatures to produce the desired mechanical properties of the neoprene compound. The neoprene layer was then heat-bonded directly to the standard aluminum panel in one piece using a multistage curing process developed at DTNSRDC. Minor surface imperfections that developed in the curing process were painstakingly repaired in order to attain a uniformly smooth surface.

The natural rubber layer was procured commercially. Before installation its surfaces were treated by a chlorination process in order to promote adhesion. A solvent-based neoprene adhesive was used to bond the natural rubber layer on the neoprene layer. The solvent was applied to both layers. The time allowed for the evaporation of the solvent before putting both layers in contact turned out to be critical. If the time allowed was insufficient, bubbles would appear between the layers. If the time allowed was too long, the result would be inadequate bonding. The correct time was found by trial and error. A few surface imperfections were observed, due to entrainment of the solvent in the final coating.

The third drag panel was comprised of a 1/4-in. thick layer of neoprene closed-cell foam bonded to the aluminum drag panel. The foam was selected on the basis of stress/strain measurements made on various foams using a strain rate of 6.35×10^{-5} m/min (0.0025-in./min). The desired stiffness was 6.9×10^{7} N/m^3 (254 lb/in.^{3}). Actual measured values for the foam ranged between 2.2×10^{7} N/m^3 (82.62 lb/in.^{3}) at 3.8 psig and 7.0×10^{8} N/m^3 (2593 lb/in.^{3}) at 75 psig. From these measurements, the shear moduli G were obtained as a function of hydrostatic pressure (see Table 1).

The neoprene foam rubber layer was bonded to the aluminum plate using the same solvent-based neoprene adhesive used to bond the natural rubber and neoprene at the last stage of the Kramer-type compliant coating. Surface microroughness was attributed to the commercial process used to slice the foam layers, which resulted in exposed open cells. In order to provide a hydrodynamically smooth layer, the surface was coated with a polyvinyl chloride paint. Absorption of the paint was so great that even after 20 coats the microroughness was still evident, which led to the conclusion that about 50% of the "closed" cells were in reality open cells. (Note that the properties reported above and in Table 1 are for the foam without the paint.)

TABLE 1 - MATERIAL PROPERTIES OF THE FOAM COATING

psig	K (lb/in.)	K/A (lb/in.^{3})	t (in.)	E (lb/in.^{2})	G (lb/in.^{2})
3.759	2.637×10^3	8.262×10^1	0.2225	18.38	6.1
9.398	5.256×10^3	1.6466×10^2	0.125	20.58	6.9
18.797	1.000×10^4	3.133×10^2	0.0825	25.85	8.6
28.196	1.714×10^4	5.371×10^2	0.0625	33.569	11.2
37.594	2.866×10^4	8.978×10^2	0.0500	44.89	15.0
46.993	3.724×10^4	1.167×10^3	0.0406	47.38	15.8
56.391	4.881×10^4	1.529×10^3	0.03375	51.60	17.2
65.790	6.524×10^4	2.044×10^3	0.028125	57.49	19.2

EXPERIMENTS

FACILITY

The experiments were performed in the 36-in. Variable Pressure Water Tunnel (VPWT) using the closed-jet test section (see Figure 2). This test section has a circular cross section of approximately 0.91 m (3.0 ft) and is 4.51 m (14.8 ft) long. A constant-speed electric motor and magnetic coupling provide about 2500 shaft horsepower (shp) to the variable pitch impeller, resulting in a maximum free-stream velocity of 24.4 m/s (80 ft/sec) in the test section. The static pressure is continuously variable from 1.38×10^4 to 4.13×10^5 N/m^2 (2 to 60 psia) independent of velocity. A pitot tube, located at the back and 20.3 cm (8 in.) above the test plate, was used to measure the free-stream velocity.

FLAT-PLATE DYNAMOMETER

The experiments were performed on a flat-plate dynamometer installed in the closed-jet test section at the horizontal midplane. The apparatus is a streamlined two-dimensional shape 307.3 cm (121 in.) long, a nominal 91.4 cm (36 in.) wide, and 7.11 cm (2.8 in.) thick. The first 25.4 cm (10 in.) from the leading edge has a NACA 16-014 shape. For the next 261.6 cm (103 in.) downstream, the apparatus is flat and parallel sided, terminated by a 21.3-cm (8.4-in.) straight-tapered trailing edge (see Figure 3). This apparatus creates a test section blockage of 10%.

The drag dynamometer consists of a frame "floating" on seven flexures, in which the sample plate is mounted flush with the surrounding surfaces, and a clevis-pin

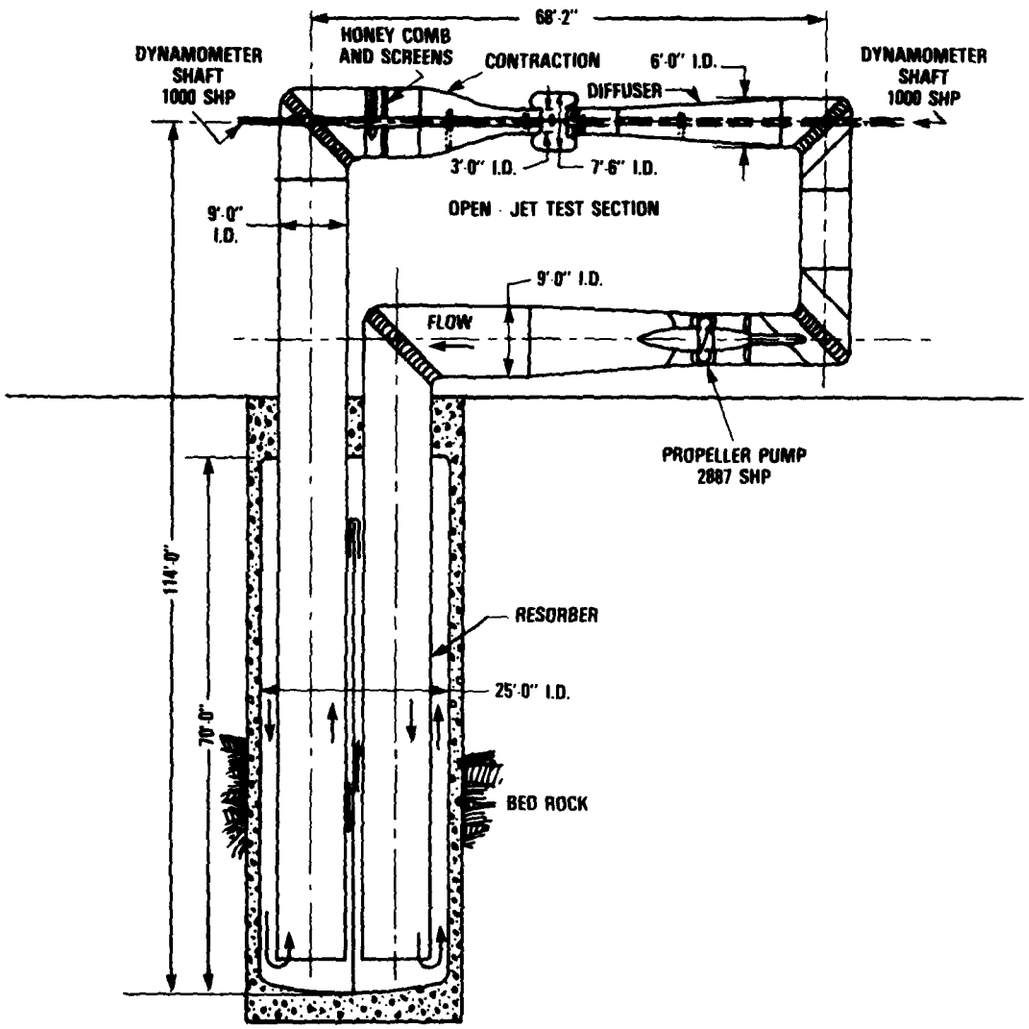

Figure 2 - Cross Section of the 36-Inch Variable Pressure Water Tunnel

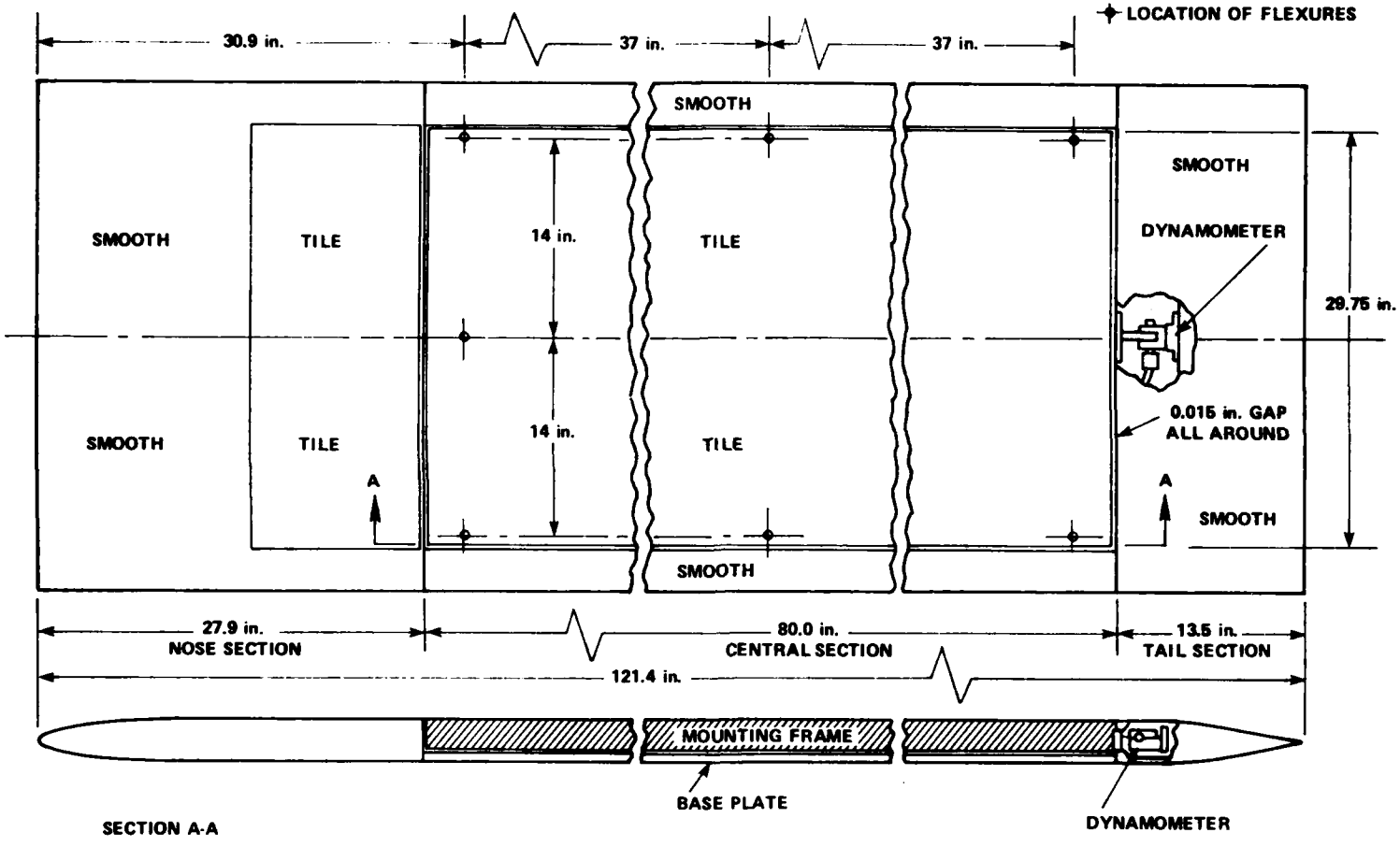

Figure 3 - Diagram of Flat-Plate Dynamometer Assembly

strain-gage transducer. The flexures restrict the motion of the floating frame to the streamwise direction only. A small gap of 0.038 cm (0.015 in.) average width isolates the frame from adjacent structures. The floating section (frame and test panel) is 203.2 cm (80 in.) long, 75.6 cm (29.75 in.) wide, and starts 70.8 cm (27.9 in.) from the leading edge of the apparatus.

In the nose section there is a 61-cm (24-in.) long removable plate. This plate can be coated with the same surface as is being tested, allowing the boundary layer to adjust to the boundary conditions in front of the drag-measuring floating section. However, for the tests reported here, only the smooth reference surface was used. The forces near the nose of the apparatus were high, and we predicted that the compliant surfaces would statically diverge, causing roughness and possible failure. The front of the short, smooth plate (9.9 cm aft of the leading edge) was shimmed up 0.025 cm (0.01 in.) to act as a trip, ensuring a fully developed turbulent boundary layer.

An assembly made with a loading sensing clevis-pin is used as the dynamometer transducer. A four-arm strain-gage bridge is sealed inside an axial hole drilled along the center line of the pin. The strain gages are located at two sections of reduced pin diameter on opposite sides of the hole on a neutral axis, ensuring that only shear forces at the gage locations will be measured. A sketch of the clevis-pin is given in Figure 4.

The clevis-pin is mounted in the forward part of the tail section as shown in Figure 3. The eye of the clevis assembly is attached to the rear of the mounting frame and the clevis is attached to the tail section. Details of the dynamometer mounting arrangement are shown in Figure 4.

TEST PANELS

During this investigation four different surfaces were used. Three were compliant coatings; the fourth was a reference, a hydrodynamically smooth surface. The reference plate was machined to a smooth surface and anodized. Both the smooth plate and the first Kramer-type compliant coating plate were leveled flush in the floating frame using shims, and then attached using counter sunk bolts through the surface. The holes were then filled with beeswax and leveled. Cutting and filling the holes in the Kramer-type coating was difficult due to the compliance of the material, and the first sample failed under test conditions, probably because of the

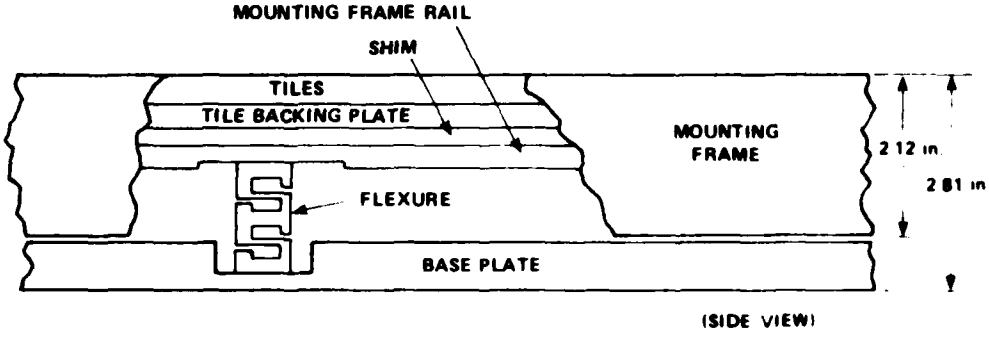

DETAILS OF FLEXURE MOUNTING (TYPICAL)

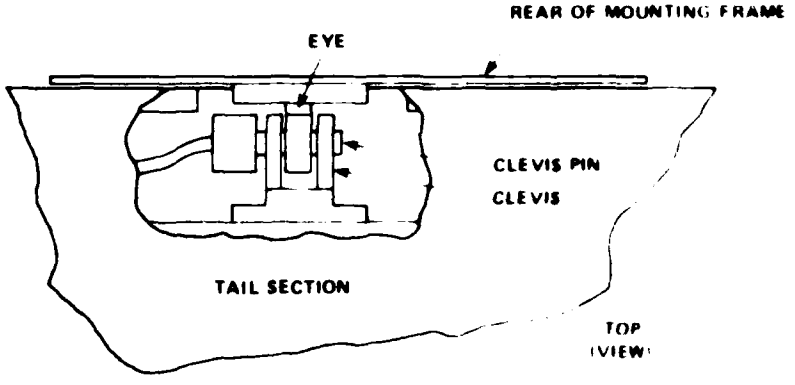

DETAILS OF DYNAMOMETER MOUNTING

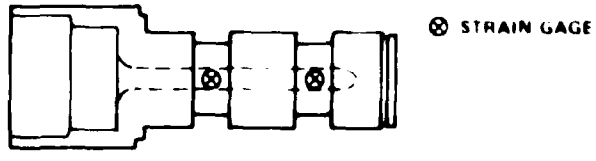

SKETCH OF CLEVIS PIN

Figure 4 - Details of Dynamometer Construction

loss of a wax plug. As a result, the apparatus was modified to allow bolting from below and the use of 24 jacking screws for leveling. The last two compliant surfaces were mounted in this manner; however, the reference plate was still bolted from the top. Vertical alignment of the panels in the frame was only constrained by the uniformity of the coating and the flatness of the backing plate.

DETAILS OF THE DYNAMOMETER DESIGN

Great care was taken in the design and manufacture of a skin-friction dynamometer. Since the drag to be measured is small, secondary forces can introduce large errors. These parasitic influences are a result of misalignment, test section pressure gradients, and flow through the floating section gaps.

Misalignment can cause the most error. The ratio of stagnation pressure force to skin-friction force is approximately 500 to 1 at high Reynolds numbers. Thus, protrusions with small frontal areas can have a large effect if they encounter high-velocity fluid. In the turbulent boundary layer, fluid speed is lower near the wall, reducing the effect of "small" misalignment. "Small" can be defined as a height that does not protrude out of the viscous sublayer which is generally considered to be in the range of 1-10 wall-length scales thick. For the present experiments at a Reynolds number of 10^7, this height is on the order of 25 μm (0.001 in.). Larger height differentials across the gap can cause flow-through and pressure buildup in the gap in addition to form drag.

In the dynamometer, the floating frame is permanently fixed in vertical alignment. This allows the edges to be custom fitted to the adjacent surfaces. The frame is designed to be as rigid as possible and is constructed out of stainless steel, as is the matching surface at the leading edge. Stainless steel is used for these precision surfaces rather than anodized aluminum to reduce damage during installation of the sample plates, some of which weigh over 45 kg (100 lb).

The leading edge of the floating frame matched the adjacent surface $\pm$50 μm with the high spots chamfered. The trailing edge was aligned to within +100 μm, -0 μm (a downward step). Along the sides (parallel to the flow) of the floating frame, vertical alignment was $\pm$300 μm (0.012 in.). This longitudinal mismatch, however, was not expected to measurably increase the drag. Substantial gains in the alignment of the floating frame-adjacent surfaces cannot be achieved with an apparatus

that can be installed in the test section without substantially increasing the flow blockage. (The apparatus breaks down into approximately ten major pieces that will fit through the hatch.)

A pressure gradient along the test section can cause a systematic bias in measurements with a flat-plate dynamometer. The test surface has internal end surfaces on which the pressure differential acts to create a force parallel to the skin drag. This force must be accounted for before the true drag is known. The ends of the floating frame had pressure taps in five locations: three aligned vertically in the center and two towards the outside (see Figure 5). No systematic difference was seen between the locations, so the central tap was used for the pressure corrections. The pressure differential (fore and aft) was then multiplied by the area of the ends to find the force, which amounted to a correction of about 5% of the total drag value. For the relatively smooth surfaces reported here, the differential pressure was essentially constant for each free-stream velocity independent of the test panel. However, for some rough surfaces, a "tare" correction term does not work.

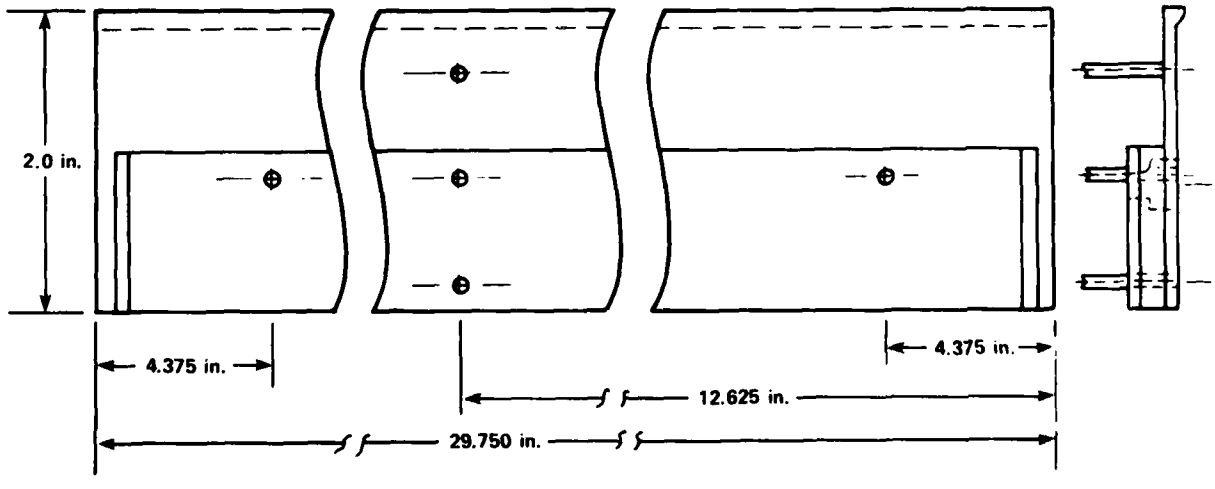

Figure 5 - Locations of Pressure Taps on the End of the Floating Frame

The size of and flow through the gap between the floating frame and the adjacent surfaces will affect the forces measured by a flat-plate dynamometer. In addition, the profile of the gap is important for minimizing errors. Allen[9] used an undercut floating element to investigate the effects of gap size, lip size, and misalignment on the forces measured by a skin-friction balance. He found that larger gaps and smaller lips decreased the sensitivity to misalignment. Small lip size decreased area for the stagnation pressure to act on before being relieved. Our apparatus was modified to reduce the effective lip size of the floating frame (see Figure 6).

Gap size has an effect on the forces exerted on the floating element. However, the mechanism of the interaction is not clearly known. To reduce the errors in a skin-friction measurement, the gap should be held constant to keep any variation systematic. Flow through the gaps can have several effects. If pressures are not equal between the plate static pressure and the dynamometer internal pressure, flow will be induced. Pressure gradients along the floating section can also cause gap flow. If an induced flow is out of the surface, modification and/or separation of the boundary layer will occur. If the flow is directed into the apparatus at the leading edge, the effect will be that of boundary layer suction. Thus, blowing or sucking will modify the flow to be measured, to some unknown extent. Flow through the gaps also means that there is flow in the apparatus.

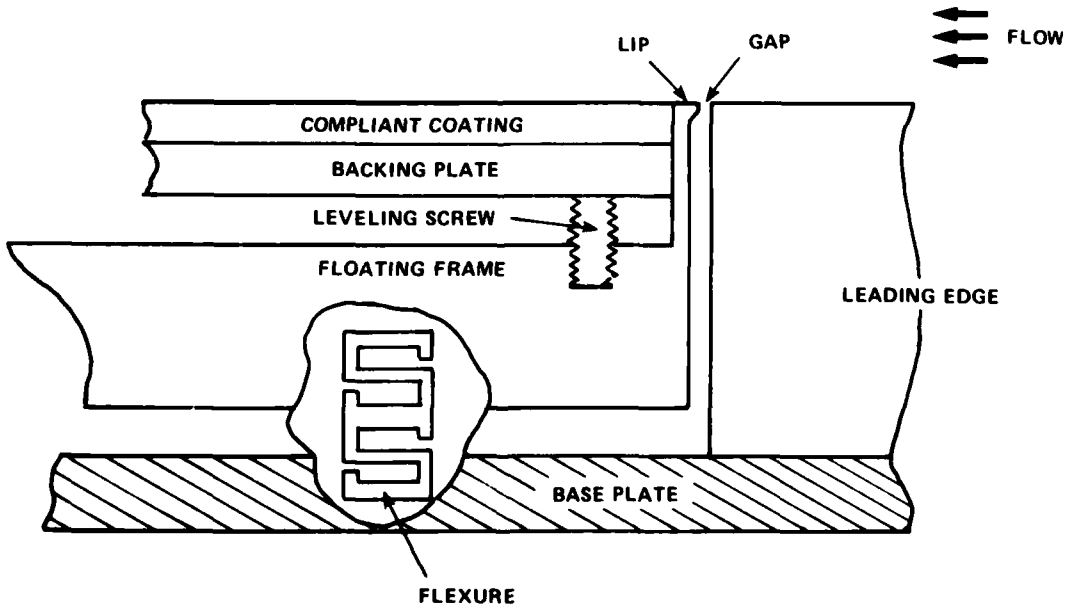

Figure 6 - Details of Gap Geometry and Leveling Arrangement

These velocities will exert an undesirable form-drag on the underside of the floating section. Thus gap flow must be held to a minimum by proper design of a flat-plate dynamometer.

ELECTRONICS

For the flat-plate dynamometer, the clevis-pin strain-gage bridge was activated, and the output signal was obtained and amplified using a voltage regulated bridge conditioner, a signal conditioner, and a differential d.c. amplifier. The bridge had a signal sensitivity of 2 mV/lb at the maximum load of 113 kg (250 lb).

Wet-wet differential (Viatran) pressure gages were used to measure both the tunnel free-stream velocity (pitot tube) and the floating frame end pressure correction. A 25-psi gage (1.75×10^5 N/m^2) was used to measure the pitot tube dynamic pressure, while a 5-psi gage (3.45×10^4 N/m^2) was used for the end pressures. These gages are supplied with built-in electronics requiring only a $\pm$15V power supply to deliver a full-scale output of $\pm$5V linearly proportional to pressure.

The dynamometer and pressure signals were low pass filtered at 5 kHz and then sampled by an Interdata Mini-Computer via an Analog to Digital converter. All data was averaged over 400 samples during a period of about 5 sec.

PROCEDURE

For all the measurements, the data was recorded at velocities between 6.1 m/s (20 ft/sec) and 18.2 m/s (60 ft/sec) using a nominal spacing of 1.5 m/s (5 ft/sec). During the runs the tunnel static pressure was set at 2.1×10^5 N/m^2 (30 psi) to prevent cavitation on the leading edge at higher velocities. The drag of the smooth plate was measured four different times--twice in the beginning, and then after each compliant coating was installed. The Preston tube measurements were taken in 1976 when the flat-plate apparatus was first built. The locations on the smooth plate where Preston tube measurements were made are shown in Figure 7.

The pressure gages were calibrated frequently between runs, using the tunnel pressure system. The dynamometer was also calibrated every time a test panel was changed. All calibration curves during these tests remained constant within 1%.

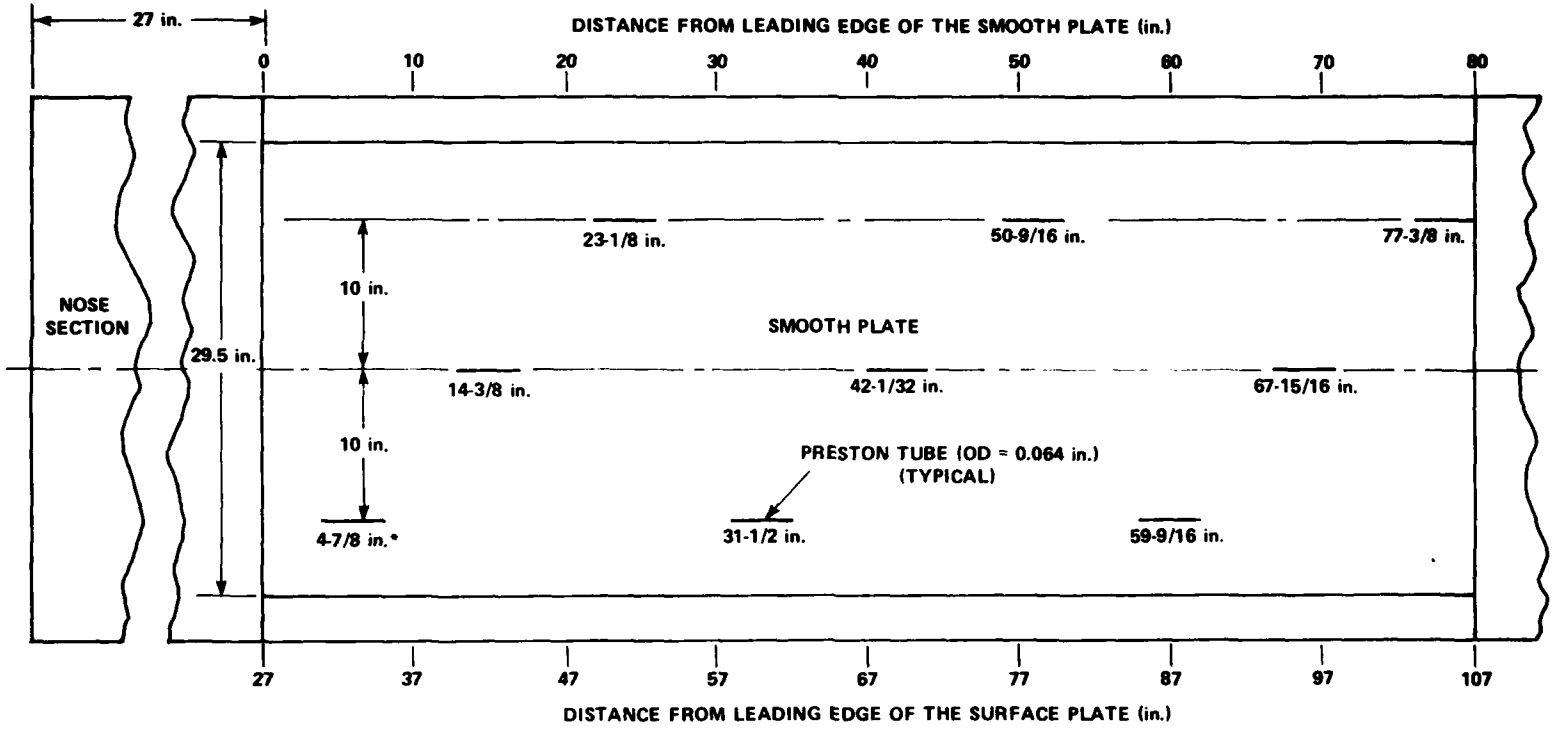

*THE DIMENSIONS WRITTEN NEXT TO THE PRESTON TUBES ARE THE DISTANCES FROM THE LEADING EDGE OF THE SMOOTH PLATE TO THE LEADING EDGES OF THE PRESTON TUBES.

Figure 7 - Location of Preston Tubes on Smooth Plate

RESULTS

SMOOTH PLATE

The results of the Preston tube measurements on the smooth plate are given in Figure 8. Here the measured local skin friction coefficient

$$c_\tau = \tau/[(1/2)\ \rho_w\ U_\infty{}^2]$$

is plotted against the Reynolds number $R_X = U_\infty\ X/\nu$; τ is the local skin friction and X is the distance from the leading edge to the measurement point. These data are compared with the Schoenherr line for local shear on a smooth plate in Figure 8 and show good agreement.

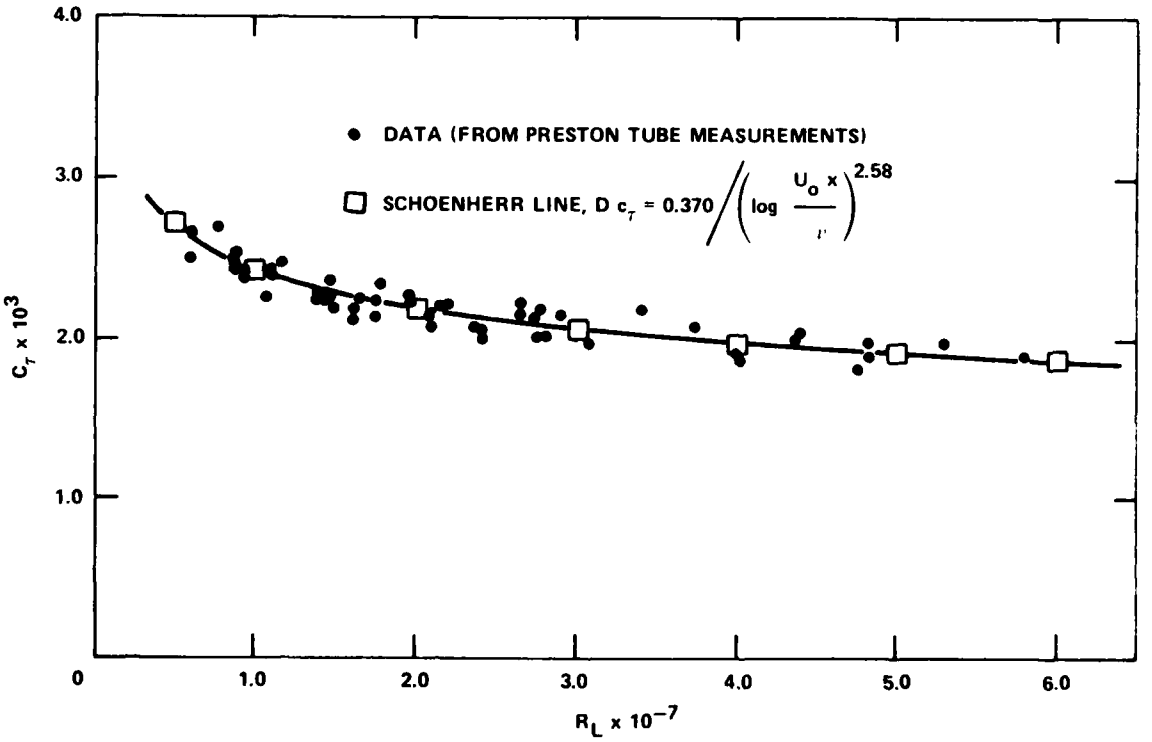

Figure 8 - Measured Flat-Plate Local Skin Friction Coefficients Compared with the Schoenherr Line

The drag data obtained from measurements of the smooth plate are presented in Figure 9. Also plotted is an "adjusted" Schoenherr friction line. In the figure, the drag coefficient

$$C_{D_2} = \frac{D_2}{(1/2)\ \rho_w U_\infty^{\ 2}\ b\ell_2} \tag{1}$$

is plotted against the Reynolds number $R_L = U_\infty\ L/\nu$, where

D_2 = drag of test plate
ρ_w = density of tunnel water
U_∞ = free-stream velocity
ℓ_2 = length of test plate
b = width of test plate
ν = kinematic viscosity of tunnel water

The Schoenherr friction line plotted in Figures 9-11 is the value of C_{D_2} obtained using Schoenherr's friction formula to obtain D_2. The Schoenherr formula assumes a turbulent flow from the leading edge and is given by

$$\frac{1}{\left(C_{D_L}\right)^{1/2}} = 4.13 \log R_L\ C_{D_L} \tag{2}$$

where

$$C_{D_L} = \frac{D_L}{(1/2)\ \rho_w\ U_\infty^{\ 2}\ bL}$$

L is the length from the leading edge of the apparatus to the rear of the test plate, and D_L is the smooth plate drag between the leading edge of the surface plate and the rear of the smooth plate. The value of D_2 is obtained from $D_2 = D_L - D_1$ where D_1 is the drag on the nose section of the surface plate. Dividing by (1/2) $\rho_w\ U_\infty^{\ 2}\ b\ell_2$ gives

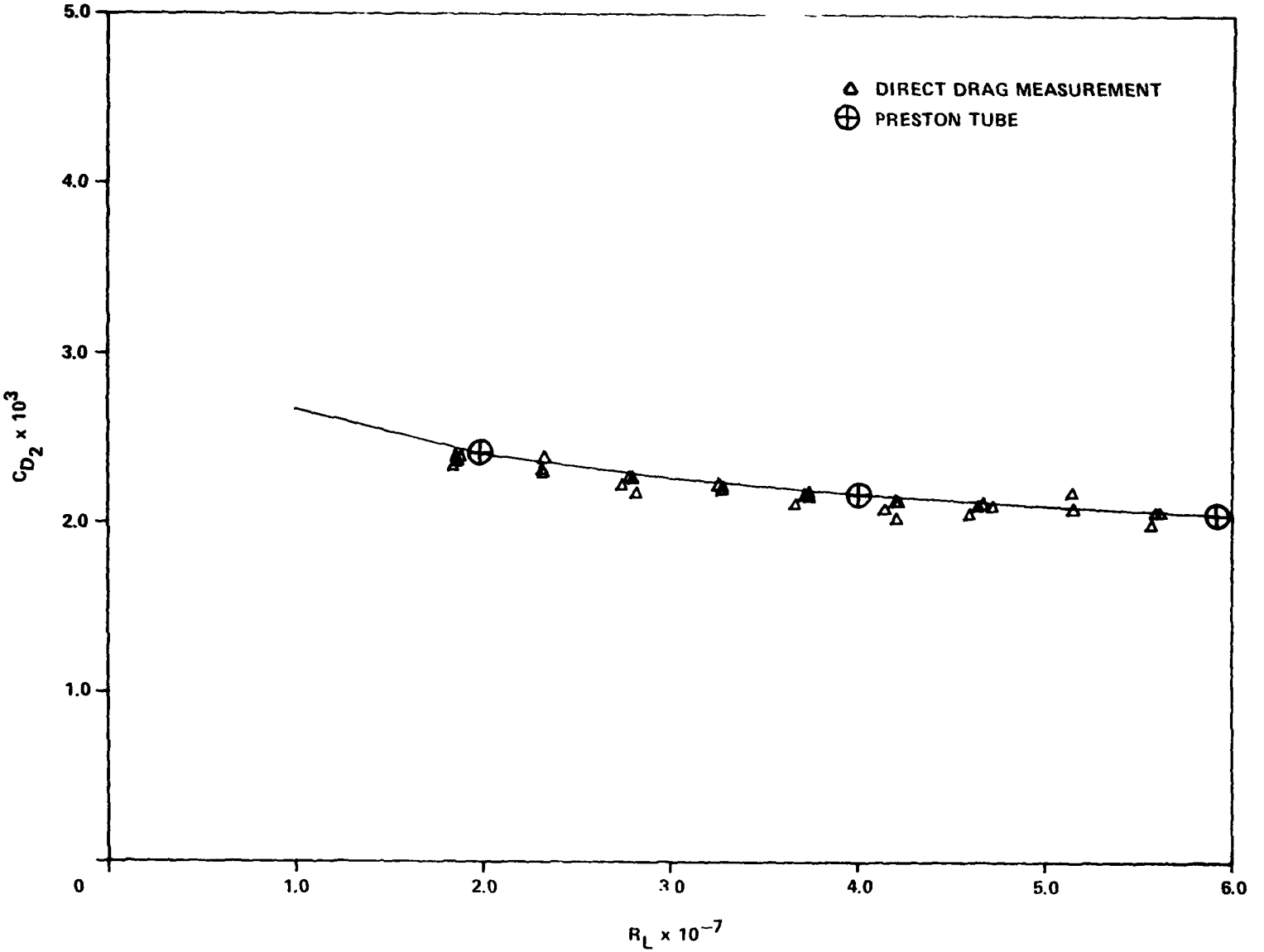

Figure 9 - Comparison of Schoenherr Equations with Measured Friction Coefficients Using Preston Tubes and the Smooth Plate

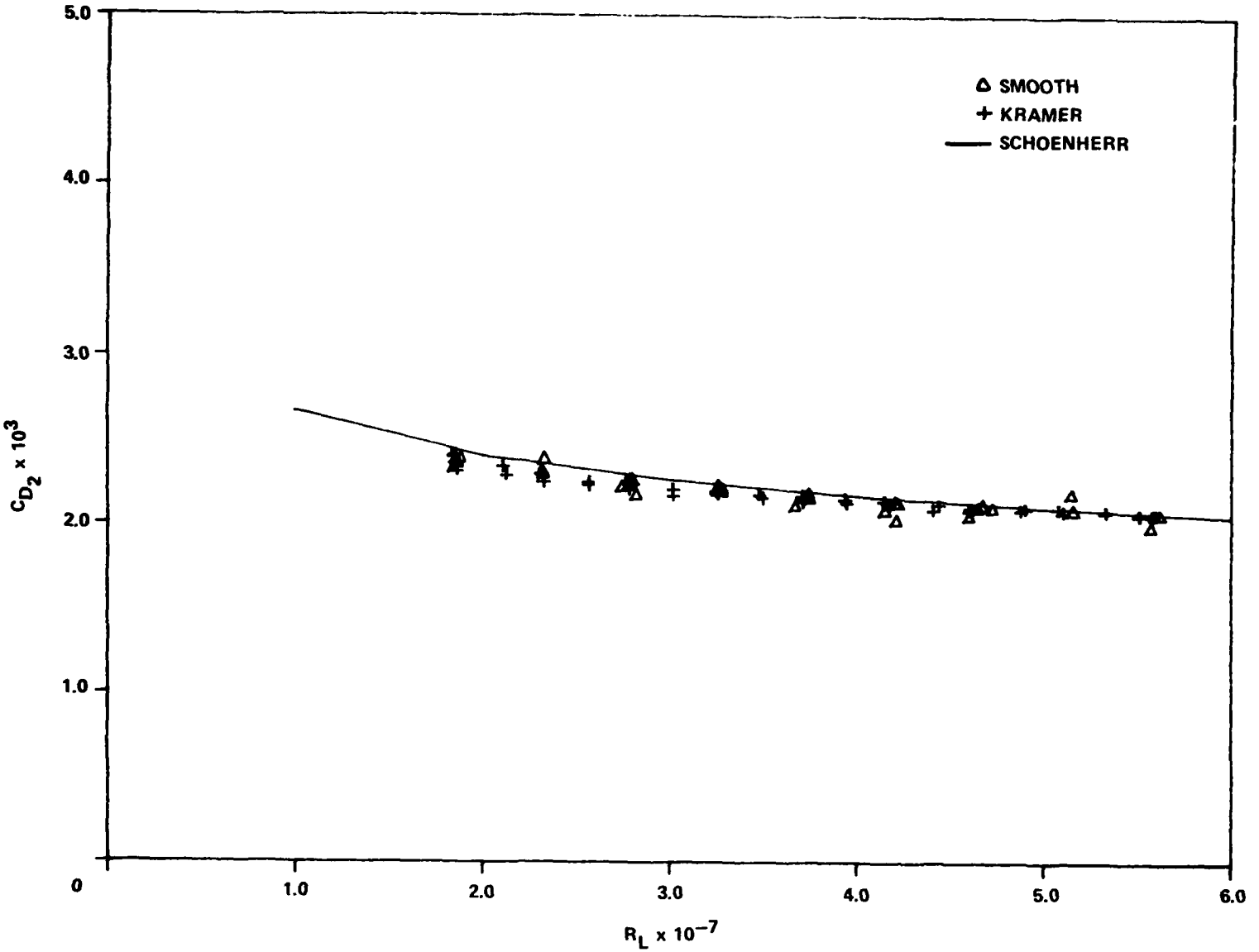

Figure 10 - Friction Coefficients of the Kramer Coating and Smooth Plate

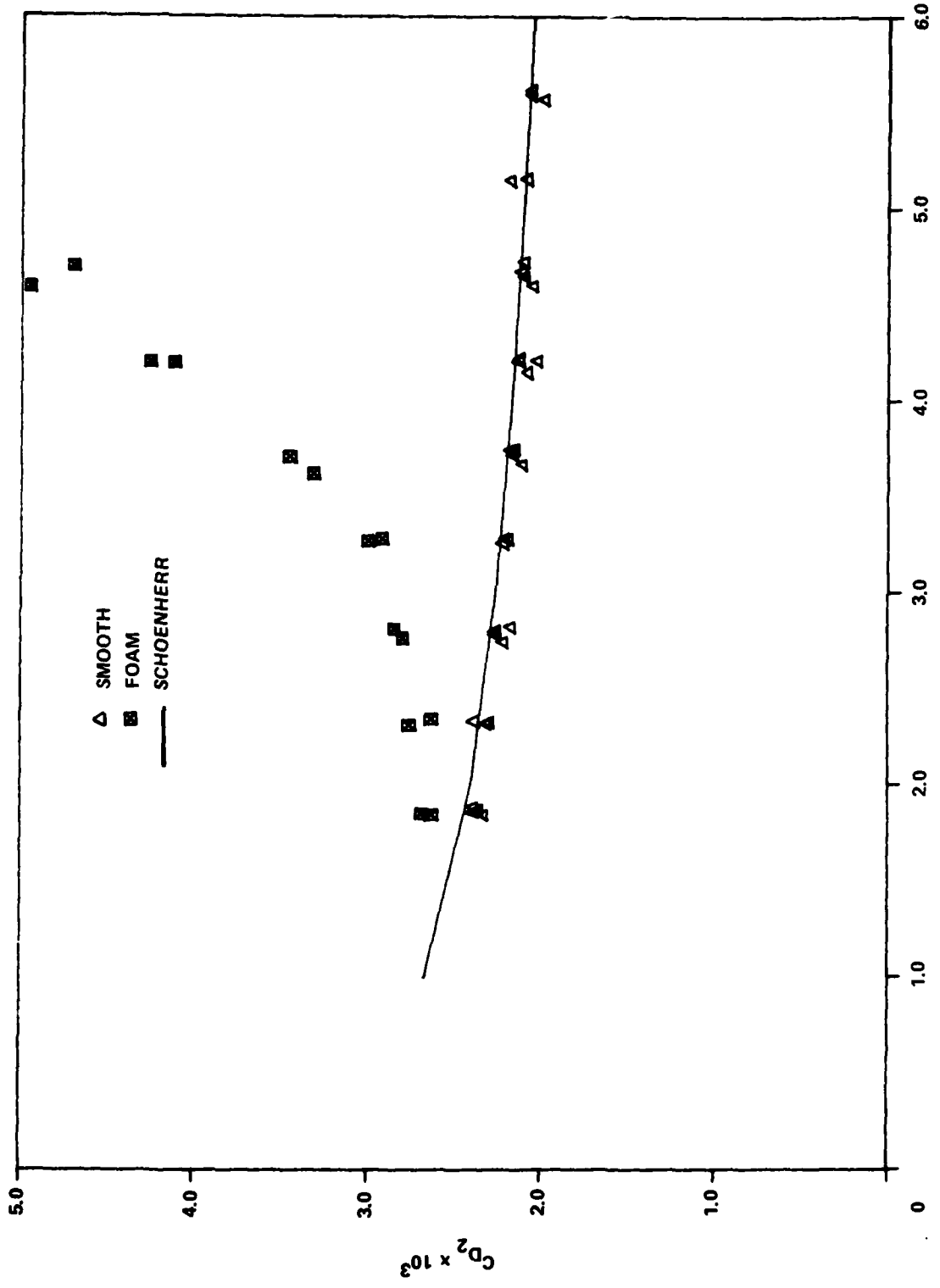

Figure 11 - Friction Coefficients of the Foam Coating and Smooth Plate

$$\frac{D_2}{1/2\ \rho_w\ U_\infty^{\ 2}\ b\ell_2} = \frac{D_L}{1/2\ \rho_w\ U_\infty^{\ 2}\ bL}\left(\frac{L}{\ell_2}\right) - \frac{D_1}{1/2\ \rho_w\ U_\infty^{\ 2}\ b\ell_2}$$

or

$$C_{D_2} = \left(\frac{L}{\ell_2}\right) C_{D_L} - \left(\frac{\ell_1}{\ell_2}\right) C_{D_1} \tag{3}$$

where ℓ_1 is the length of the nose section. Both C_{D_L} and C_{D_1} are obtained from Equation (2) as functions of R_L and R_{ℓ_1}, respectively, where

$$R_{\ell_1} = U_\infty\ \ell_1/\nu$$

Using the results from Figure 8, the total drag coefficient of the smooth plate

$$C_{D_2} = \left(\frac{1}{\ell_2}\right) \int_{\ell_1}^{L} c_\tau\ (X)\ dx$$

was computed using the measured values of c_τ. The computations were made at three values of R_L, and the results are plotted in Figure 9. The computed values for C_{D_2} from the Preston tube data, the values from the adjusted Schoenherr friction line, and the measured drag values for the smooth plate all agree well.

From the discussion of errors affecting the flat-plate dynamometer, one should not be surprised to find a systematic difference between the adjusted Schoenherr line and the measured drag. While in the data reported here the agreement is good, the dynamometer has been installed and used four previous times, and the measured drag of the smooth plate has been up to 5% above the Schoenherr line. For any particular installation, however, the measurements have been repeatable. For this project the root mean square scatter of the data about a local mean is 2%. Due to

the possibility of a systematic error in the apparatus, comparisons between test panels are referenced to the actual measured value of the smooth plate rather than to an empirical Schoenherr friction curve.

KRAMER COATING

The Kramer-type coating was a two-layer coating, as discussed previously. In the first experiment (1981) the coating was torn apart at 9.1 m/s (30 ft/sec). However, with the present manufacturing process, our sample survived flows up to 18.3 m/s (60 ft/sec). The only other modification to the drag panel was a piece of plastic tape wrapped around the leading portion to prevent the flow from striking the slightly irregular edge. The surface in general had a smooth microfinish, but there were large-scale irregularities as mentioned above.

The drag on the Kramer coating was measured at intervals of 0.76 m/s between 6.1 and 18.3 m/s. The results are shown in Figure 10. There was no measurable difference in drag between the compliant surface and the rigid, smooth plate. The rms scatter in the data is also about 2%.

FOAM COATING

The closed-cell neoprene foam coating was pressure sensitive, compressing in size and increasing in bulk modulus with increasing pressure. We had hoped to obtain a range of bulk moduli by varying the tunnel pressure; however, misalignment with the adjacent surfaces restricted measurements to pressures near atmospheric pressure. The foam never had a smooth surface because of the open cells at the surface, despite many coats of paint.

The drag of the foam coating was measured at intervals of 1.5 m/s from 6.1 to 15.2 m/s where the drag reached the maximum of the clevis-pin strain gage. The results are shown in Figure 11. The drag at the lower Reynolds numbers is greater than that for the smooth plate, probably due to the rough surface. Starting at a Reynolds number of about 3.5×10^7, the drag increases rapidly. Transverse waves were observed on the coating at this point. Figure 12 shows the waves at a free-stream velocity U_∞ = 12.2 m/s (40 ft/sec). These waves are similar to those reported by Hansen et al.[10] and indicate static divergence.

The scatter of the data increases with tunnel velocity. The coating had a time lag between the application of a mean pressure and the response of the bulk modulus.

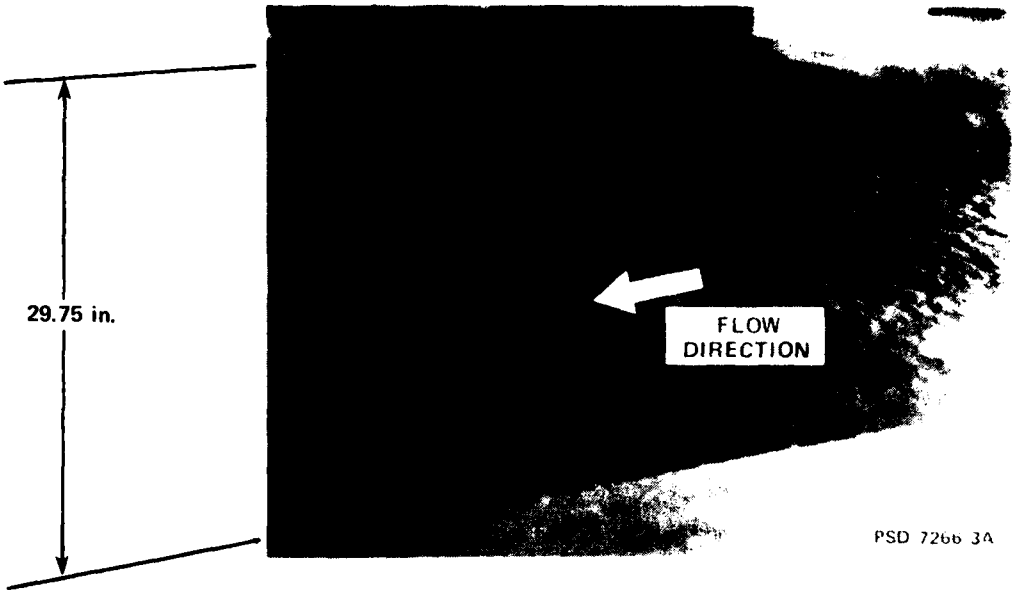

Figure 12 - Static Divergence Occurring on the Foam Coating
(U_{∞} = 40 ft/sec)

During static divergence, the waves grew with time at a constant water velocity, but due to the concern over possible coating breakup, the present experiments were run quickly at the higher Reynolds numbers. This caused scatter of the data.

MATCHING THE PROPERTIES OF A COMPLIANT COATING TO A TURBULENT BOUNDARY LAYER

At the present time no complete theory has been developed to explain the interaction between turbulent flow and a compliant structure. The following model, though highly simplified, is proposed to provide some rationale for selecting materials and experimental conditions in the search for drag-reducing coatings.

The model starts with the fact that the turbulent boundary layer exerts fluctuating pressures on the material surface. The surface responds to these pressures by becoming deformed, with a resultant normal surface velocity. This surface velocity interacts back into the turbulence via the change of boundary condition, we hope reducing the turbulent momentum transport toward the surface. The reduced transport of streamwise momentum should then reduce the local shear and wall skin friction. In this whole process the wall must be maintained as hydraulically smooth, because form drag will negate any shear stress reductions.

We are interested in high-speed applications using "passive" coatings, wherein a turbulent boundary layer acts on a material surface which is not forced (no external energy input). No additives to the working fluid are considered, so the constitutive equation for the turbulent flow is that of a Newtonian fluid.

The effect that the fluid region will have on the solid, and vice versa, takes place through the boundary conditions. First we have velocity boundary conditions. Requiring that the wall be impermeable yields

$$\underline{u} \cdot \hat{n} = \underline{U} \cdot \hat{n}$$

where $\underline{U}$ is the wall velocity, $\underline{u}$ is the fluid velocity, and $\hat{n}$ is the unit vector normal to and pointing out of the wall. The normal velocities of both the fluid and the wall must be the same at the wall. The no-slip boundary condition can be expressed as

$$\underline{u} \times \hat{n} = \underline{U} \times \hat{n}$$

If we do not allow the wall to move tangentially, the fluid velocities at the wall and parallel to it must be zero.

The force boundary conditions must also be examined. Since the fluid acts on the wall in the same way that the wall acts on the fluid, if the fluid is not going to experience infinite acceleration at the wall, the stresses must be continuous across the boundary. The tangential viscous stresses must be matched at the wall, and to the first order there are no normal viscous stresses. However, the normal pressure force per unit area must be continuous across the wall.

In matching the turbulent flow properties to the coating properties, the boundary conditions must be considered. With light and sound, impedance matching has worked well for liquid/solid boundaries. By analogy we attempt an impedance matching for compliant surfaces-turbulent boundary-layer interaction. Impedance measurements are routine for the characterization of rubbers, so the compliant material part of the exercise presents no problems. However, how does one characterize a turbulence impedance? Within the framework of the model stated earlier, the normal forces and velocities are the important parameters. Thus, to characterize the turbulence impedance we will try to estimate the significant pressure forces and normal velocities of the turbulent flow at the wall.

Let us first examine the compliant coating. The parameters that define the coating are as follows:

Parameter [Dimensions]	Name
G [Force/area]	Shear modulus
K [Force/displacement]	Dynamic stiffness
A [Area]	Area of sample tested (length × breadth)
T [Length]	Thickness of coating
ρ_c [Mass/volume]	Density of coating
ω_o [Time^{-1}]	Resonance frequency of coating

We will let ω_o be the independent variable since this is the value measured by the impedance tester; A, T, and ρ_c will be constants since they can be chosen in manufacture. Therefore, we need two equations to define the material.

The first equation

$$\frac{K}{A} = \frac{\rho_c T \omega_o^2}{3} \tag{4}$$

defines the dynamic stiffness of the coating, and the second equation

$$\frac{K}{A} = \frac{G}{T} \tag{5}$$

relates the normal to the shear properties of the coating. Thus

$$\frac{K}{A} = \frac{G}{T} = \frac{\rho_c T \omega_o^2}{3} \tag{6}$$

Likewise we can list the parameters defining the turbulent boundary layer:

Parameter [Dimensions]	Name
P' [Force/area)	Significant pressure fluctuation ("footprint" pressure)
k_a [Length]	Admissible roughness of a hydraulically smooth surface
U_∞ [Length/time]	Free-stream velocity

c_τ	[None]	Friction coefficient
ρ_w	[Mass/volume]	Water density
ν	[Length^2/time]	Kinematic viscosity of water
ω	[Time^{-1}]	Frequency of significant pressure fluctuations
δ	[Length]	Boundary layer thickness
X	[Length]	Distance from leading edge to dynamometer

Since we wish to design for a coating at a specified velocity let us keep U_∞ as the independent variable; ρ_w, ν_w, and X will be constants. We are left with five dependent variables and thus need five equations for a closed problem. At this point some assumptions must be made about the turbulent flow. We are trying to understand how to design a real coating and to understand the relationship between the flow and the desired coating. Thus, we will use proportionality in many of these equations when the actual constants are not well known so we can get a physical feeling for the nature of the modeled interaction. Actual estimates will be made further along in this report.

$$P' \propto \frac{\rho_w U_\infty^2}{2} \tag{7}$$

$$k_a \propto \bar{\lambda} = \frac{\nu}{(c_\tau/2)^{1/2} U_\infty} \quad (\bar{\lambda} \text{ is the wall flow length scale; from Schlichting}^{11} \text{ page 659}) \tag{8}$$

$$\omega = \frac{3 U_\infty}{\delta} \quad (\text{from Blake}^{12} \text{ and Bull}^{13}) \tag{9}$$

$$\delta = 0.37 X \left(\frac{U_\infty X}{\nu}\right)^{-1/5} \quad (\text{from Schlichting}^{11} \text{ page 638}) \tag{10}$$

and

$$c_\tau = f(R_X) \tilde{=} \text{constant (assumed)} \tag{11}$$

The assumption in Equation (8) is justified, since at our large Reynolds number c_τ is a weak function of Reynolds number or a constant within the accuracy of the other assumptions. Using Equation (10) in Equation (9) to eliminate δ, we obtain for the frequency response

$$\omega = \frac{3\ U_\infty^{6/5}}{(0.37)\ \nu^{1/5}\ X^{4/5}} \tag{12}$$

Recalling that our two boundary conditions are pressure and normal velocity, let us scale these with the available parameters. The pressures that cause a response in the coating are those associated with the turbulent bursting events or the "footprints." For this condition we will use P' as the significant pressure fluctuations. The normal velocity that we desire at the surface is associated with motion of maximum amplitude (before the surface becomes rough) and it occurs at the frequency of the significant pressure fluctuations. Thus, the average velocity scale will be $\omega k_a/\pi$.

Using the pressure and velocity scales based on the fluid boundary conditions, we can form a "turbulence impedance:"

$$Z_T = \frac{\pi P'}{\omega k_a} \tag{13}$$

We see that this is similar to the normal specific acoustic impedance for an elastic solid.

$$Z_A = \frac{Z_M}{A} = \frac{\sqrt{KM}}{A} = \sqrt{(K/A)\rho_c T}$$

But

$$\frac{K}{A} = \frac{\rho_c\ T\ \omega_o^{\ 2}}{3} \quad \text{(from Equation (4))}$$

Thus

$$Z_A = \frac{\rho_c T \omega_o}{\sqrt{3}} \tag{14}$$

If we match impedances

$$Z_A = Z_T$$

$$\frac{\rho_c T \omega_o}{\sqrt{3}} = \frac{\pi P'}{\omega k_a} \tag{15}$$

which gives us the condition for which we wish to design the compliant coating. Using Equations (7)-(12), we find

$$\rho_c T \omega_o \propto X^{4/5} c_\tau^{1/2} \rho_w \nu^{-4/5} U_\infty^{9/5} \tag{16}$$

$$Z_A \propto U_\infty^{9/5} \tag{17}$$

for fixed values of X, c_τ, ρ_w, and ν.

A different matching of the flow to the compliant coating illuminates a further constraint on design. Matching forcing conditions yields

$$\frac{K}{A} = \frac{P'}{k_a} \propto \frac{\rho_w U_\infty^3 c_\tau}{\nu}$$

or

$$K \propto U_\infty^3 \tag{18}$$

for fixed ρ_w, ν, and c_τ.

However, if we match the resonance frequency of the coating to the frequency of the significant pressure fluctuations, we find

$$\omega_o = \omega \propto \frac{U_\infty^{6/5}}{\nu^{1/5} X^{4/5}}$$

But, since, by Equation (6),

$$K \propto \omega_o^2$$

it follows that

$$K \propto U_\infty^{12/5} \tag{19}$$

It is immediately obvious that we can meet the conditions of Equations (18) and (19) only at one free-stream velocity. This agrees with our initial prediction based upon the argument that while forces causing the deflection are going up, the roughness limit goes down.

In addition to the boundary condition matching, there is a constraint on the minimum shear modulus of the compliant coating. This constraint is due to the phenomenon of static divergence. Transverse waves form above a maximum free-stream velocity reported by Hansen et al.,[10] to be

$$U_\infty > 3.3 \left(\frac{G}{\rho_w}\right)^{1/2} \tag{20}$$

for rotating disks. For the foam coating tested, the numerical value was 1.9. Combining Equations (6) and (20) and using a value of 3.3 yields

$$\frac{K}{A} > \frac{U_\infty^2 \rho_w}{10\ T} \tag{21}$$

creating a physical constraint on the type of compliant coating that can exhibit drag reduction within the assumption made above.

REGIONS OF IMPEDANCE MATCHING

The impedance matching technique introduced in the last section is highly simplified. At the present time no "complete" theory has been developed to explain the interaction between a turbulent flow and a compliant structure. Thus experimental models are ahead of analytical techniques. However, the need exists for a rational selection of flows and materials to be used for experiments, so a simple model is valuable.

The model proposed uses the coating operating at resonance. In an actual environment this condition may not be met. Are there other conditions which may be more advantageous? For example, all phase information has been ignored. Is the phase relationship between the fluid forcing and the material response important? These questions will be examined qualitatively in this section.

The relation between the impedance and frequency for a compliant rubber material is complex (see Figure 13 and Plunkett[14]). At low frequencies (below resonance) the material behaves like a spring, while at high frequency the coating operates as a mass. Around resonance both the spring and the mass properties are important. As the frequency goes from low to high, the phase angle, between the pressure force and

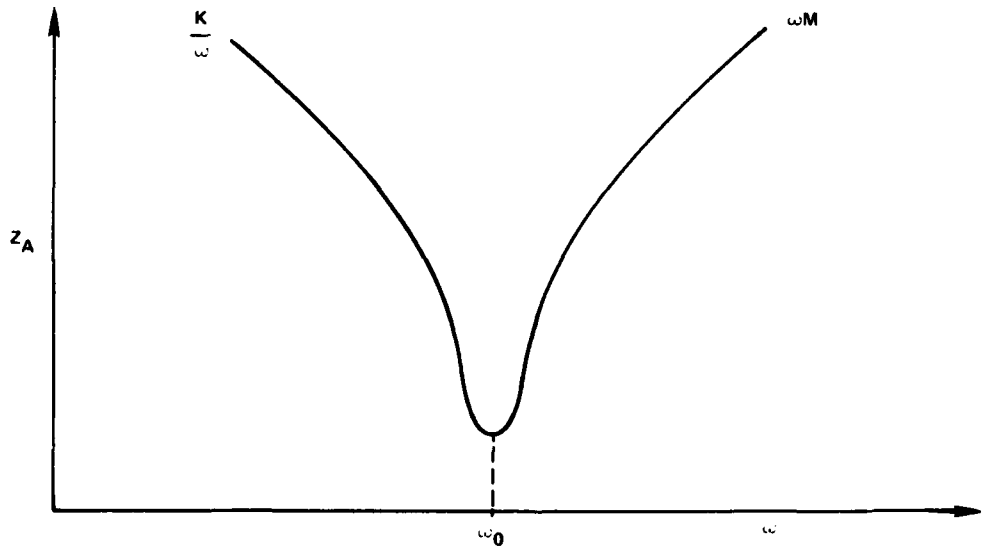

Figure 13 - Specific Acoustic Impedance Z_A versus Frequency ω for a Rubber Compliant Coating

the compliant surface displacement, goes from 0 to π (see Figure 14). The phase angle is $\pi/2$ at the resonant frequency with the pressure leading the displacement. Since the impedance matching model uses the velocity of the fluid-compliant material interface, we note that the pressure leads the velocity from $\pi/2$ to $3\pi/2$ as the frequency increases.

Over the limited range of Reynolds numbers available in a water tunnel, the turbulence impedance versus frequency curve is approximately linear with a positive slope. Figure 15 shows the computed turbulence impedance for a Naval Ocean Systems Center Water Tunnel.[7] Figure 15 corresponds to the case of holding the geometry of a flat plate constant and varying the free-stream velocity. The impedance is shown graphically as a zone since the turbulence actually has a spectrum of frequencies, and the scaling used in the analysis is empirical.

There are three distinct ways in which the turbulence impedance can be matched to the coating impedance. First, the impedance can be matched at the material resonance (Figure 16a). In this case there will be a region of overlap, the area of which will vary according to the losses in the compliant coating. At resonance the velocity of the interface will lag behind the turbulent pressure by 180°. If the pressure fluctuations are periodic and caused by "bursts" and "sweeps," the interface will be moving upward under the high-pressure burst (being ejected) and downward under the low-pressure sweep. This would appear to be a positive feedback causing increased turbulence levels. Whether impedance matching at resonances will increase or decrease drag is not known; however, the material will respond most efficiently to the turbulence, so this case is the one which is most likely to produce a measurable change.

Second, the impedance can be matched below the compliant coating resonance frequency (Figure 16b). In this case there will be a small area of overlap. The interface velocity should lag behind the pressure fluctuation's lag by approximately 90°. The coating will not operate as efficiently as at resonance; however, the chances of getting the impedance to intersect experimentally are greater, as may be seen qualitatively by comparing Figures 16a and 16b.

The third way to match impedance is above resonance (Figure 16c). Since both impedances have positive slope in this region, the area of matching can be large. As the velocity of the vehicle goes up, the impedances would remain matched and the coating would be effective over a larger range of operating conditions. However,

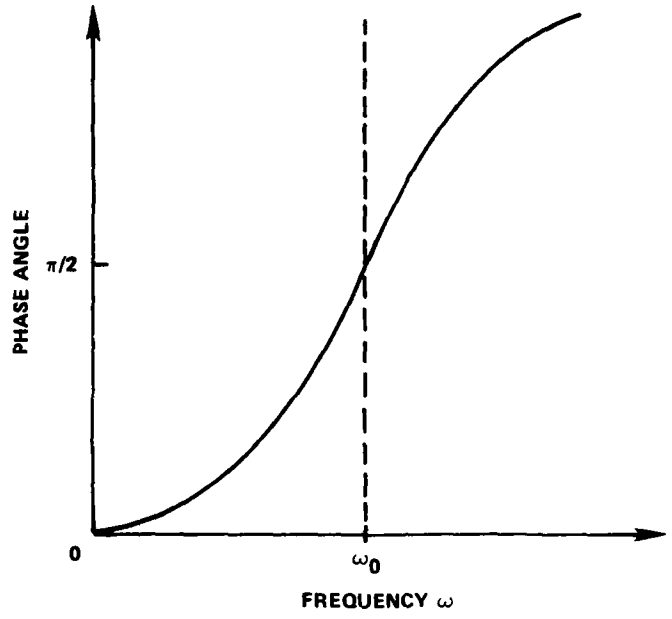

Figure 14 - Phase Angle Between the Pressure Forcing Function and the Displacement of a Compliant Surface

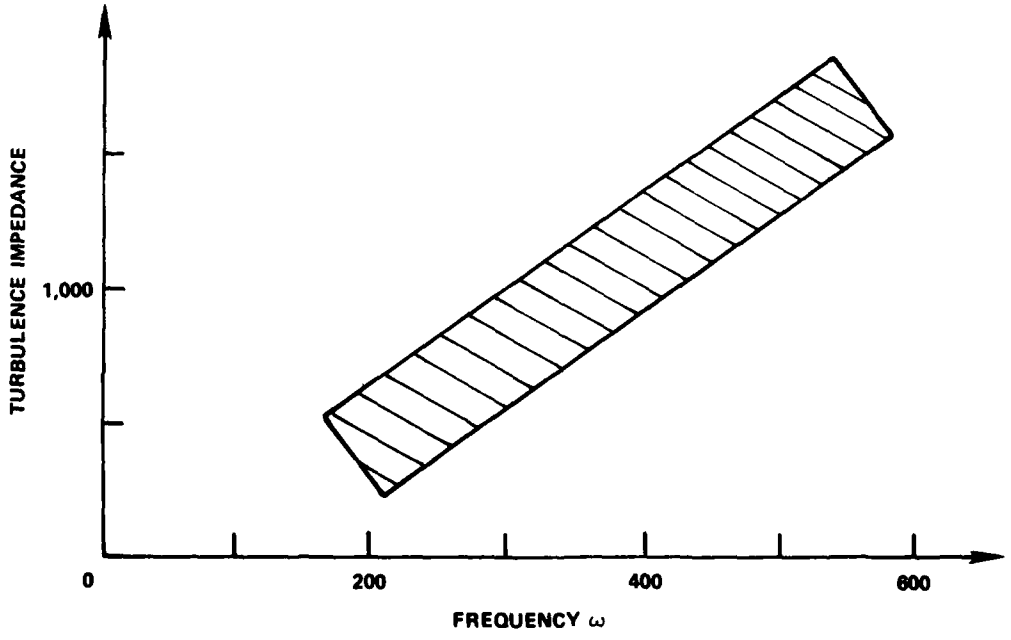

Figure 15 - Turbulent Impedance versus Frequency for a Boundary Layer as the Velocity is Varied

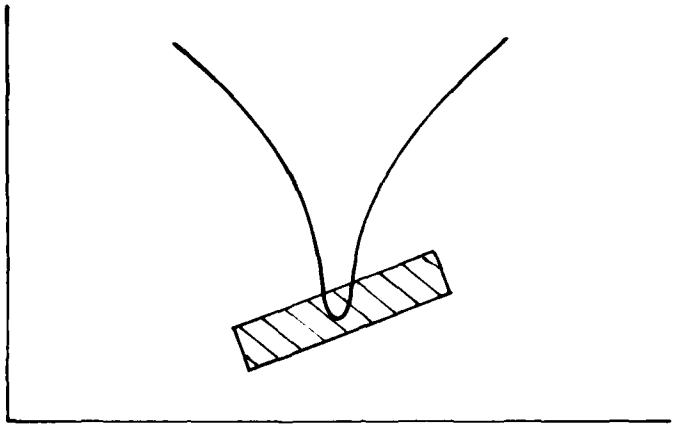

Figure 16a - At Resonance

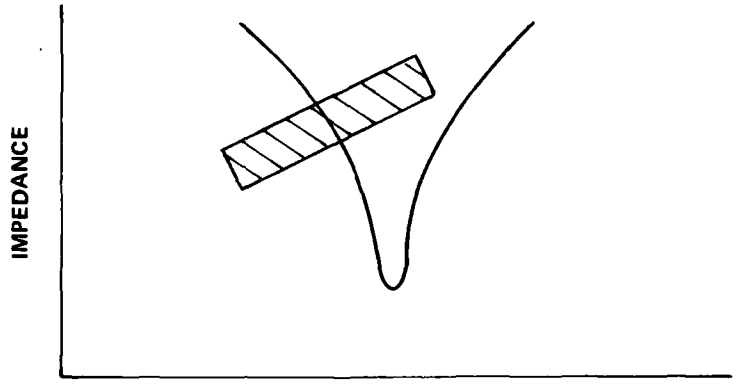

Figure 16b - Below Resonance

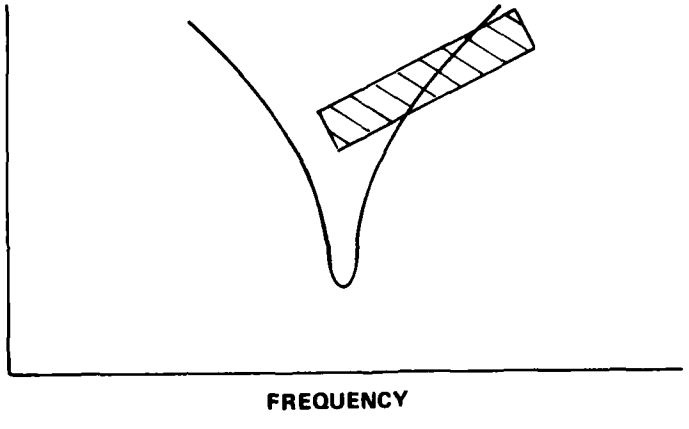

Figure 16c - Above Resonance

Figure 16 - Impedance Matching Between the Turbulence and the Compliant Coating

the properties would have to be carefully matched since the chance of intersection of impedances is reduced, as may be qualitatively seen when comparing Figures 16b and 16c. Above resonance the pressure could lead the interface velocity by as much as 270°. In a periodic pressure field the velocity would lead by 90° and perhaps provide negative feedback to the burst-sweep process. Again, however, the coating will not respond as efficiently as at resonance.

DESIGN OF AN ACTUAL COATING

This is the hypothetical design for a coating to be tested in the DTNSRDC 36-in. water tunnel. The coating will operate at a velocity of 30 knots (15.24 m/s), have the same thickness as the Kramer coatings, and be made of a rubber material.

Constants for the flow will be $\rho_w = 1$ g/cm^3, $\nu = 0.01$ cm^2/sec, $U_\infty = 1524$ cm/sec, $c_\tau = 0.0022$ assumed, and $X = 274.3$ cm.

$$\frac{\rho_c T \omega_o}{\sqrt{3}} = \frac{\pi P'}{\omega k_a}$$

We must determine P', ω, and k_a to determine material properties:

$$P' = 0.005 \rho_w U_\infty^2/2 = 5806.4 \text{ dynes/cm}^2 \text{ (from Bull}^{12}\text{)}$$

$$\omega_o = \frac{3 U_\infty^{6/5}}{(0.37) \nu^{1/5} X^{4/5}} = 1506 \text{ rad/sec} = 240 \text{ Hz}$$

and

$$k_a = 5\overline{\lambda} = 5 \frac{\nu}{(c_\tau/2)^{1/2} U_\infty} = 0.00094 \text{ cm (from Schlichting}^{11}\text{ pages 657-665)}$$

Therefore

$$\frac{\rho_c T \omega_o}{\sqrt{3}} = 12{,}885 \text{ grams/cm}^2 \text{ sec}$$

or, with $\rho_c = 1$ gm/cm^3 and T = 0.254 cm,

$$\omega_o = 87{,}861 \text{ rad/sec} = 13{,}983 \text{ Hz}$$

The density and thickness were selected to be similar to the Kramer coating--as a result $\omega_o > \omega$. This is impedance matching below resonance (discussed in the last section).

Using Equation (4) and the static divergence constraint for a transverse-wave-free coating (Equation (18)) with the inequality reversed, we obtain

$$\left(\frac{5\rho_c}{\rho_w}\right)^{1/2} T\,\omega_o \geq U_\infty \tag{22}$$

Plugging in the values for our example,

$$49{,}902 \text{ cm/sec} \geq U_\infty = 1524 \text{ cm/sec}$$

so this constraint is satisfied.

CONCLUSIONS

The ability to produce and to measure the drag of large size compliant coatings at DTNSRDC has been demonstrated. A new design method for compliant coatings is introduced by developing a turbulence impedance and matching it with the specific acoustic impedance of the coating. Three possible matching regions are presented and discussed.

The following conclusions can be drawn on the basis of the present investigation:

- The coatings reported here did not reduce drag.
- Static divergence is a constraint for real coatings and must be considered in the design process.
- An impedance matching technique has been developed for the design of experimental compliant coatings. Experiments are needed to evaluate the matching process and to confirm whether drag reduction is possible.

ACKNOWLEDGMENTS

The authors would like to thank Mr. Armando Santiago for his painstaking efforts in producing the coatings. The discussions with Dr. Thomas Huang during the progress of this work were of great benefit.

REFERENCES

1. "Drag Reduction Symposium," Washington, D.C., sponsored by the Office of Naval Research, the National Aeronautics and Space Administration, the Air Force Office of Scientific Research, and the Naval Sea Systems Command (1982).

2. Kramer, M.O., "Boundary Layer Stabilization by Distributed Damping," ASNE Journal, Vol. 72, pp. 25-33 (Feb 1960).

3. Kramer, M.O., "The Dolphins Secret," ASNE Journal, Vol. 73, pp. 103-107 (Feb 1961).

4. Kramer, M.O., "Boundary Layer Stabilization by Distributed Damping," Navy Engineers Journal, Vol. 74, pp. 341-348 (May 1962).

5. Kramer, M.O., "Boundary Layer Control by 'Artificial Dolphin Coating,'" Navy Engineers Journal, Vol. 89, pp. 41-45 (Oct 1977).

6. Klebanoff, P.S., N.E. Mease and W.R. Rowland, "An Experimental Investigation of Drag Reduction with Compliant Surfaces," Drag Reduction Symposium, National Academy of Sciences, Washington, D.C. (13-17 Sep 1982).

7. Rathsom, A., G. Mastny, T. Phillips, and M. Reischman, "Deformation Measurements on Compliant Surfaces," Drag Reduction Symposium, National Academy of Sciences, Washington, D.C. (13-17 Sep 1982).

8. Madigosky, W.M., "Coating Fabrication and Characterization," Compliant Coating Drag Reduction Program Review, Washington, D.C. (14-15 Oct 1981).

9. Allen, J.M., "Improved Sensing Element for Skin-Friction Balance Measurements," AIAA Journal, Vol. 18, No. 11 (1980).

10. Hansen, R.J., D.L. Hunston, C.C. Ni and M. Reischman, "An Experimental Study of Flow-Generated Waves on a Flexible Surface," Journal of Sound and Vibration, Vol. 68, pp. 317-334 (1980).

11. Schlichting, H., "Boundary-Layer Theory," (Seventh Ed.) McGraw-Hill Book Co., New York (1979).

12. Blake, W.K., "Turbulent Boundary-Layer Wall-Pressure Fluctuations on Smooth and Rough Walls," Journal of Fluid Mechanics, Vol. 44, Part 4, pp. 637-660 (1970).

13. Bull, M.K., "Wall Pressure Fluctuations in Turbulent Flow," Journal of Fluid Mechanics, Vol. 28, Part 4, pp. 719-754 (1967).

14. Plunkett, R., "Mechanical Impedance," Department of the Navy, Bureau of Ships Report No. 375-N-31 (1958).

INITIAL DISTRIBUTION

Copies		
2	ONR	
	1	432 (C. Lee)
	1	432 (M. Reischman)
2	NRL	
	1	5844 (R. Hansen)
	1	Lib
5	NAVSEA	
	1	SEA 55N (Shelton)
	1	SEA 55W3 (W. Sandberg)
	1	SEA 55N2 (A. Paladino)
	1	SEA 56XP (F. Peterson)
	1	SEA 63R31 (T. Peirce)
2	NSWC, White Oak	
	1	Lib
	1	R31 (W. Madigosky)
2	NOSC, San Diego	
	1	6341 (Rathsam)
	1	Lib
12	DTIC	
2	NASA, Langley	
	1	Bushnell (Mail Stop 163)
	1	Lib
4	NBS	
	1	Hunston (Polymer Division)
	1	Klebanoff (Chemical Process Metrology Div.)
	1	Mease
	1	Lib
2	Johns Hopkins Univ./APL	
	1	APL-Lib
	1	APL-Taylor
2	Pennsylvania State Univ.	
	1	Merkle (Dept., Mechanical Eng.)
	1	ARL-Lib
2	Flow Research Co.	
	1	Duncan-Silver Spring, MD
	1	Gad-el-Hack-Kent, WA

Copies	
1	Science Applications, Inc Annapolis, MD C. Von Kerczek

CENTER DISTRIBUTION

Copies	Code	Name
1	012.2	B.V. Nakonechny
1	15	W.B. Morgan
1	154	J. McCarthy
1	1540	P. Granville
1	1542	T. Huang
25	1542	S. Dickinson
3	1542	J. Power
1	1905	W. Reader
1	1908	R. Rippeon
1	1965	M. Tracy
3	2842	J. Eynck
10	5211.1	Reports Distribution
1	522.1	TIC (C) + 1 (m)
1	522.2	TIC (A)

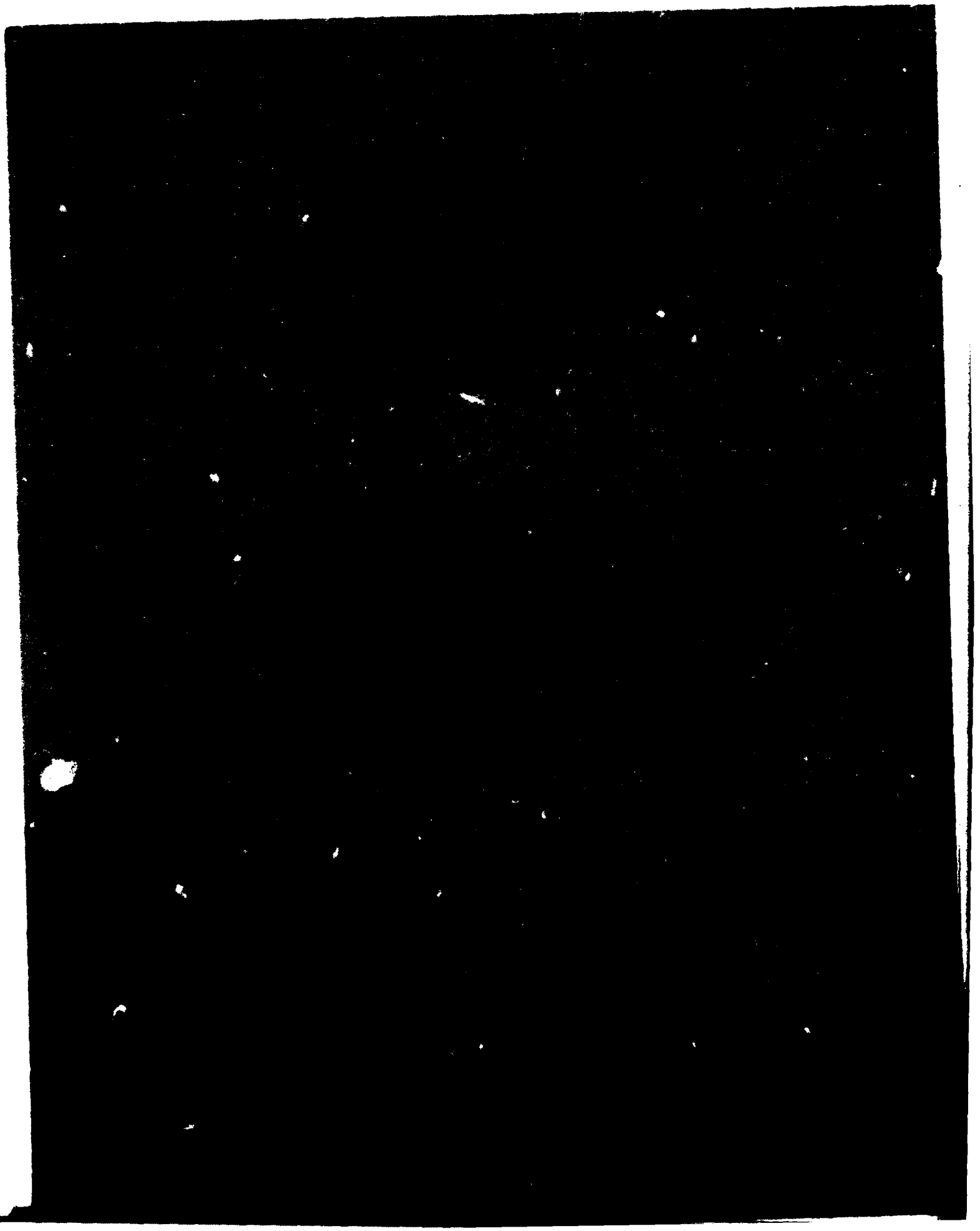


N L
ATE
LME